

Continuous propagation and energy filtering of a cold atomic beam in a long high-gradient magnetic atom guide

Spencer E. Olson,* Rahul R. Mhaskar, and Georg Raithel

FOCUS Center, Physics Department, University of Michigan, Ann Arbor, Michigan 48109-1120, USA

(Received 28 July 2005; revised manuscript received 23 November 2005; published 29 March 2006)

We demonstrate the continuous injection and propagation of a cold atomic beam in a high-gradient (up to 2.7 kG/cm) magnetic guide of 1.7 m length. Continuous injection is accomplished using a side-loading scheme that involves a sequence of two modified magneto-optic traps. Methods are developed to measure the atomic-flow temperatures and the flux under steady-state conditions. In the high-gradient portion of the guide, the guided atomic beam has a transverse temperature of $420 \mu\text{K} \pm 40 \mu\text{K}$, a longitudinal temperature of 1 mK, and an average velocity of order 1 m/s. Using a radio-frequency current of a fixed frequency ν coupled directly into the guide wires, atoms exceeding a transverse energy of $h\nu$ can be continuously and selectively removed from the atomic beam.

DOI: [10.1103/PhysRevA.73.033622](https://doi.org/10.1103/PhysRevA.73.033622)

PACS number(s): 03.75.Be, 03.75.Dg, 32.80.Pj

I. INTRODUCTION

In atom interferometers, relative phase shifts of de Broglie matter waves can be utilized to measure atomic accelerations due to electromagnetic fields [1], gravitational fields [2], rotations [3], and interactions with other atoms [4,5]. The recent surge of interest in atom interferometry stems from this wide range of potentially detectable phenomena and the associated high precision due to the short de Broglie wavelength of matter waves in the velocity range of interest (from $\lesssim 1$ m/s to a few 10 m/s) [6]. One approach to build atom-interferometric devices is based on the use of magnetic atom guides, which provide narrow, conservative guiding potentials for cold atoms. In analogy with fiber-optic interferometers, which are commonly operated using lasers, guided-wave atom interferometers will presumably operate best with an atom source that injects a monochromatic continuous flow of cold atoms into the lowest transverse mode of the atom guide. However, just as white-light optical interferometry is possible using nearly matched optical path lengths, precise atom interferometry may be possible using a reasonably monoenergetic beam of atoms [7]. In this paper, we report on a continuous cold atomic beam that could be further developed for atom-interferometric applications. The beam is prepared in a magnetic atom guide of 1.7 m length and a transverse gradient up to 2.7 kG/cm. The number of guide modes that significantly contribute to the atom flux is controlled by energy-selective atom filtering, enabled via a continuously applied radio-frequency current. We characterize the beam by a complete set of temperature and flux measurements.

II. OVERVIEW OF THE EXPERIMENTAL SETUP

Our experimental setup consists of two laser-cooling stages that prepare atoms for a high-gradient magnetic atom guide. Atoms, first collected in a vapor-cell pyramidal magneto-optical trap (PMOT in Fig. 1), are transferred into

and recaptured by a secondary MOT (MMOT in Fig. 1). This MMOT then injects the atoms into the 1.7-m-long magnetic atom guide with a tunable velocity. As shown in Fig. 1, the guide is comprised of a vertical injection and launch section (about 0.2 m height) and a horizontal section (1.5 m length) in which rf-induced transitions are employed to selectively remove the most energetic atoms from the guided atomic flow.

The magnetic atom guide consists of a pair of in-vacuum hollow copper tubes with an outer diameter of 3.18 mm and a center-to-center separation as low as 4.18 mm. The copper tubes are introduced into the vacuum chamber through Swage-Lok feedthroughs with Teflon ferrules and are precision-mounted in the vacuum on a steel rail using alumina, aluminum spacers, and polyimide foil (see inset of Fig. 1). The mounts are designed such that a well-defined tube separation is achieved as a function of the longitudinal position in the magnetic guide. The aluminum-polyimide mounts are sufficiently loose so as to allow the tubes to slide longitudinally. This is necessary to provide relief for thermal expansion, which can be up to ~ 1 mm under normal operating conditions. The steel rail on which the guide tubes are mounted provides stability and rigidity to the structure. Long, periodic slots in this steel rail allow optical access to the region between the guide tubes. A precision machined rail surface minimizes washboardlike gravitational bumps along the length of the guide. The hollow guide tubes are cooled using a closed-circuit, high-pressure water flow. At a current of 300 A, the magnetic-field gradient reaches values of 2.7 kG/cm, generating accelerations of 90 g on ^{87}Rb atoms in the state $|F=1, m_F=-1\rangle$. The system is routinely operated using the continuous-mode parameters listed in Table I.

III. ATOMIC-FLOW INJECTION

A. Primary atomic beam: Side-loading the MMOT

The primary atomic beam used to load the atom guide is generated by the PMOT [8], a fluorescence image of which is shown in Fig. 2. Our PMOT, operated with a single laser

*Electronic address: Spencer.E.Olson@umich.edu; <http://cold-atoms.physics.lsa.umich.edu>

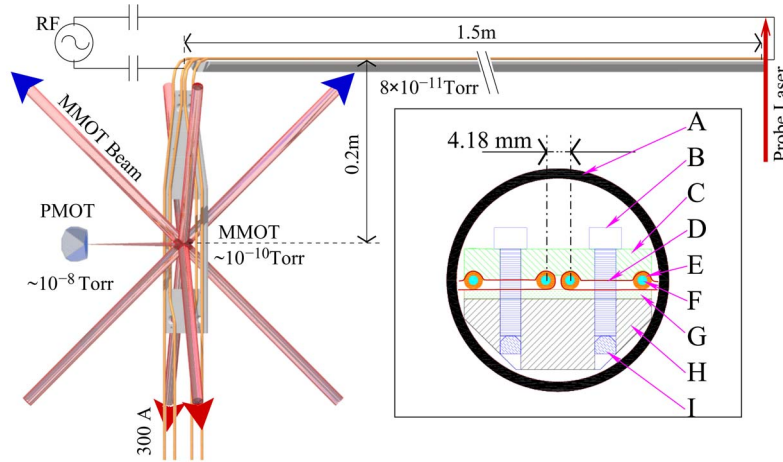


FIG. 1. (Color online) Sketch of the experimental setup. Atoms are injected from a pyramidal magneto-optical trap (PMOT) via a “moving MOT” (MMOT) into the vertical injection and launch section of a magnetic atom guide. As the injected atomic flow rises upward, it slows under the influence of gravity and becomes magnetically compressed. The flow then propagates into a long horizontal guide section. A radio-frequency current coupled into the horizontal guide section is used to remove the most energetic atoms from the guided atomic flow. The system has three differentially pumped vacuum regions, the pressure values of which are shown here. The inset on the right shows a cross section through the horizontal section of the guide. (A) Vacuum chamber, (B) mounting screws, (C) aluminum spacers, (D) insulating polyimide film, (E) guide wires, (F) coolant, (G) alumina spacers, (H) guide rail, and (I) lock screws.

beam with a bandwidth of <2 MHz full width at half maximum (FWHM) and 100 mW power, is a version of the MOT [9] that emits a cold atomic beam through a hole in the apex of a pyramidal mirror [10]. This is similar to a low-velocity intense source (LVIS [11]) of atoms. To initiate the atomic beam from the PMOT, the atom cloud in Fig. 2 is centered over the apex of the pyramid using a tunable-bias magnetic field. The resultant imbalance in radiation pressure causes the atoms to be extracted through the indicated exit hole in the form of a freely propagating atomic beam.

To characterize the unguided beam emitted from the PMOT, we have performed a series of absorption measurements. As depicted in Fig. 3, a low-intensity ($\sim 0.15I_{\text{sat}}$ with saturation intensity $I_{\text{sat}} = 1.6 \text{ mW/cm}^2$), small-diameter, near-resonant probe beam was arranged to intersect the PMOT atomic beam at an angle $\theta = 45^\circ$ in the vicinity of the MMOT. The spatial profile of the PMOT atomic beam was determined by measuring the absorption for different vertical positions of the probe beam. To determine the velocity distribution, for each vertical position y the probe laser was scanned across the atomic absorption resonance and the absorption was measured as a function of the laser frequency.

TABLE I. Parameters of continuous-mode operation of the magnetic atom guide.

Guide current	300 A
Field gradient (end of guide)	2.7 kG/cm
Dissipated power	3.2 kW
Cooling water pressure	120 PSI
Water inlet temperature	16 °C
Water temperature differential	30 °C
Vacuum pressure (horizontal guide region)	8×10^{-11} Torr

Due to the Doppler effect, the laser detuning from resonance, $\delta\nu$, and the velocity of the atoms, v_z , are approximately related by $(v_z/\lambda)\cos\theta$. This allows us to plot the absorption due to the PMOT atomic beam as a function of vertical position and velocity. The data, shown in Fig. 4, yield an average velocity of the primary atomic beam $\langle v_z \rangle = 22 \text{ m/s}$ and a FWHM spread of $\Delta v_z = 16 \text{ m/s}$. The FWHM spread of the absorption signal in height is $\Delta y = 16 \text{ mm}$. Since the distance between the PMOT and MMOT is about 16 cm, the full angular spread of the primary beam is about 100 mrad.

The flux Φ_{PMOT} of the atomic beam is determined as follows. In the limit of weak absorption, the absolute power $dP(y, \nu_L)$ absorbed by the PMOT atomic beam from the small probe beam is given by

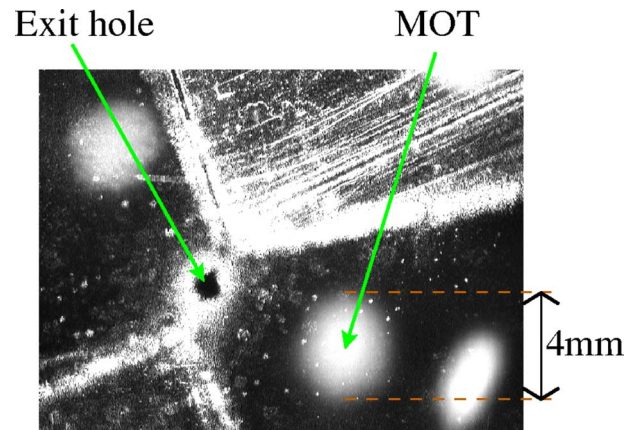


FIG. 2. (Color online) Primary pyramidal MOT (PMOT). The image shows the actual atom cloud and multiple reflections thereof in the pyramidal mirror.

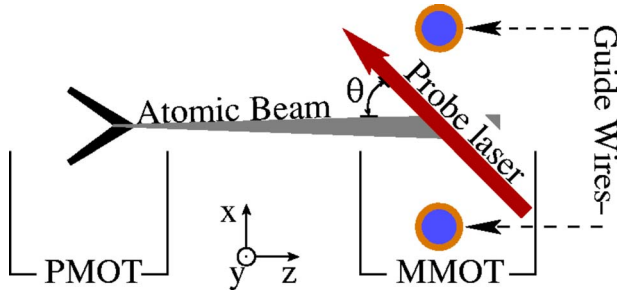


FIG. 3. (Color online) Setup of absorption measurement used in order to characterize the (unguided) primary atomic beam emitted by the PMOT. The current in the guide wires is turned off for this measurement.

$$\begin{aligned} dP(y, \nu_L) &= -h\nu_L \int_{-\infty}^{\infty} N(y, v_z) \gamma(v_z, \nu_L) dv_z \\ &= -h\nu_L \int_{-\infty}^{\infty} N(y, v_z) \frac{\Gamma}{2} \left(\frac{II_{\text{sat}}}{1 + 4\left(\frac{2\pi\delta}{\Gamma}\right)^2} \right) dv_z, \end{aligned} \quad (1)$$

where ν_L is the laser frequency, γ is the velocity- and frequency-dependent photon scattering rate, Γ is the line-width ($2\pi \times 6$ MHz), I is the laser intensity, and $I_{\text{sat}} = 1.6$ mW/cm². $N(y, v_z)$ is the number of atoms in the probe beam per velocity element dv_z at height y . The dependence of dP on ν_L is also contained in the atom-field detuning δ seen by the atoms,

$$\delta = \frac{\cos(\theta)}{\lambda} v_z + \nu_0 - \nu_L, \quad (2)$$

where ν_0 is the unshifted frequency of the atomic transition. Noting that the probe-beam diameter is much smaller than the atomic-beam diameter, the fractional absorption $dP(y, \nu_L)/P$ is

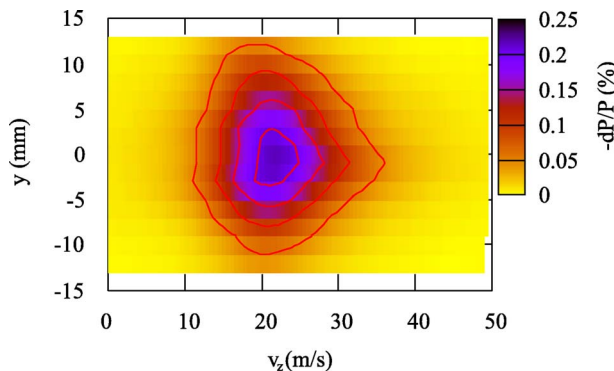


FIG. 4. (Color online) Contour plot of the relative absorption $-dP/P$ due to the primary atomic beam as a function of vertical position y and velocity v_z .

$$\begin{aligned} \frac{dP(y, \nu_L)}{P} &= -\frac{h\nu_L \Gamma}{2I_{\text{sat}}} \int_{-\infty}^{\infty} \left(\frac{N(y, v_z)}{A} \right) \frac{1}{1 + 4\left(\frac{2\pi\delta}{\Gamma}\right)^2} dv_z \\ &= -\frac{h\nu_L \Gamma}{2I_{\text{sat}}} \int_{-\infty}^{\infty} \left(\frac{n_A(y, v_z)}{\sin(\theta)} \right) \frac{1}{1 + 4\left(\frac{2\pi\delta}{\Gamma}\right)^2} dv_z, \end{aligned} \quad (3)$$

where A is the probe-beam cross section and $n_A(y, v_z)$ is the number of atoms per area element $dydz$ and per velocity element dv_z ; i.e., n_A has units of $\text{m}^{-2}(\text{m/s})^{-1}$. Using the reasonable assumption that $n_A(y, v_z)$ does not vary much over the velocity range over which the second factor under the integral in Eq. (3) is significant, we may replace $n_A(y, v_z)$ by $n_A(y, v_R)$, where

$$v_R = \frac{\lambda}{\cos \theta} (\nu_L - \nu_0) \quad (4)$$

is the velocity of atoms for which the probe laser beam is on resonant—i.e., for which $\delta=0$ in Eq. (2). The integral can then be calculated, yielding

$$n_A(y, v_R) = -\frac{dP(y, \nu_L(v_R))}{P} \frac{4I_{\text{sat}} \sin(2\theta)}{hc\Gamma^2}. \quad (5)$$

Denoting the peak absorption by $(dP/P)_0$ and the peak value of n_A by n_0 , it is $n_0 = -(dP/P)_0 4I_{\text{sat}} \sin(2\theta) / hc\Gamma^2$. Noting that the volume density of atoms, $n_V \approx n_0 \Delta v_z / \Delta x$, and assuming that the PMOT atomic beam is symmetric about its axis (i.e., the FWHM spreads of the atomic beam $\Delta x = \Delta y$), the estimated atomic flux is

$$\begin{aligned} \Phi_{\text{PMOT}} &\approx n_V \Delta x \Delta y \langle v_z \rangle \\ &= n_0 \Delta v_z \Delta y \langle v_z \rangle \\ &= -\frac{4I_{\text{sat}}}{hc\Gamma^2} \left(\frac{dP}{P} \right)_0 \Delta v_z \Delta y \langle v_z \rangle, \end{aligned} \quad (6)$$

where $\theta = \pi/4$ has been used. Using the measurement result $(dP/P)_0 = -0.22\%$ and the above values for the average velocity, the velocity spread, and the height of the PMOT beam, we find $\Phi_{\text{PMOT}} \approx 3 \times 10^9 \text{ s}^{-1}$. Due to the approximations made in the analysis, we expect the result to be accurate to within 30% of the stated value. It was also observed that the flux for higher PMOT laser powers was higher. For example, a PMOT laser power of 130 mW resulted in a flux of around $5.3 \times 10^9 \text{ s}^{-1}$.

B. Injection into the magnetic guide

The atomic beam emitted by the PMOT propagates into the differentially pumped UHV ($\sim 10^{-10}$ Torr) section of the setup that contains the vertical portion of the atom guide. As seen in Fig. 1, the horizontal atomic beam emitted by the PMOT side-loads the vertical injection and launch section of the atom guide at a right angle. The injection into the guide is accomplished using a MMOT [12,13]. As shown in Fig. 1, the four coplanar copper tubes that provide the magnetic

guiding fields throughout most of the apparatus also create the two-dimensional magnetic quadrupole field necessary for the MMOT. The inner tubes are spaced at a center-to-center distance $a_1=3.7$ cm and carry parallel currents, while the outer tubes are spaced at a distance $a_2=5.7$ cm and provide the current return path. For a current of $I=300$ A, the radially symmetric field gradient near the guide axis,

$$\frac{\partial B}{\partial \rho} = \frac{4\mu_0 I}{\pi} \left[\frac{1}{a_2^2} - \frac{1}{a_1^2} \right], \quad (7)$$

is about 20 G/cm at the location of the MMOT. Four laser beams are directed at the intersection point of the atomic beam incident from the PMOT with the vertical launch section of the guide. All beams are aligned at an angle of 45° relative to the vertical guide axis. As Fig. 1 shows, the four MMOT beams consist of a pair with upward and a pair with downward directions. The planes spanned by these beam pairs are orthogonal to each other and contain the vertical axis. The beams with downward direction are operated at a slightly lower frequency than those with upward direction. The MMOT beams are red detuned from the $^{87}\text{Rb } 5S_{1/2} F=2 \rightarrow ^{87}\text{Rb } 5P_{3/2} F'=3$ transition by an amount $\delta_{\text{MMOT}} \sim 2\Gamma$. The beams are circularly polarized in a suitable manner and have intensities of about 5 mW/cm². This configuration of magnetic fields and laser beams results in a two-dimensional MMOT that compresses the divergent atomic beam emitted by the PMOT into a small-diameter cylindrical region (~ 200 μm) around the guide axis (which is vertical in the launch section). The average velocity v_0 (=launch velocity) of the atoms leaving the MMOT is parallel to the guide axis and can be tuned by varying the frequency difference of the up-going and down-going MMOT beams. In the frame of reference of the moving atoms, the frequencies of the MMOT are Doppler shifted such that all beams appear at the same frequency. Thus, $v_0 = \epsilon\lambda/\cos(\theta)$, where ϵ is half the frequency difference between the up-going and down-going beams, λ is the wavelength of the atomic transition (780.244 nm), and $\theta=45^\circ$ is the angle between the MMOT beams and the vertical. Typically, the relative detuning is adjusted such that the MMOT launches the atoms at $v_0 = 2.2$ m/s, which is within the range of velocities where MMOTs have proven to operate well [14–18].

An absorption scheme similar to the PMOT characterization was implemented to determine the performance of the MMOT as a function of detuning and gradient. In this case, because of limited optical access, the probe beam had to be aligned perpendicular to the atomic flow and the guide field naturally had to be on. While these boundary conditions prevented us from measuring the velocity distribution, the output flux of the MMOT could be determined using the method explained in the following.

A low-power ($\sim 0.15I_{\text{sat}}$), circularly polarized probe laser beam was aligned to intersect the topmost portion of the MMOT, just before the extraction zone. The diameter of the probe was made appreciably larger than the diameter of the atom flow in the MMOT. The MMOT was run in a pulsed fashion in which the MMOT light was on for 88 ms. During this time, the probe laser was off and atoms were cooled into

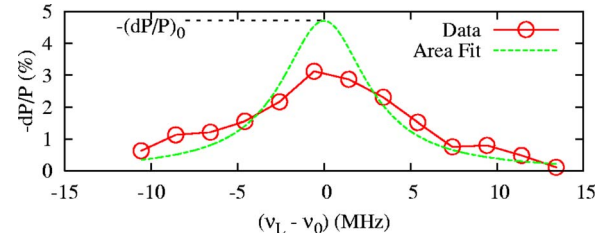


FIG. 5. (Color online) Relative absorption $-dP/P$ of a probe beam passed through the atomic beam exiting the MMOT vs the frequency detuning of the probe laser, $\nu_L - \nu_0$. The red circles show measured data, while the green line shows a Lorentzian of 6 MHz FWHM that has the same area as the data curve.

the moving reference frame of the MMOT until steady-state conditions were reached. After the MMOT light was switched off, the probe laser was turned on and the relative absorption dP/P observed immediately after the turn-on of the probe was recorded. This procedure was repeated for different probe-laser frequencies ν_L .

For simplicity, we first consider the case where Zeeman effects can be neglected. In this case, the absolute power dP absorbed from the probe laser is, in the limit of weak absorption, given by

$$dP = -N\gamma h\nu_L = -N\frac{\Gamma}{2} \frac{III_{\text{sat}}}{1 + 4\left(\frac{2\pi\delta}{\Gamma}\right)^2} h\nu_L, \quad (8)$$

where N is the number of atoms in the probe beam and $\delta = \nu_L - \nu_0$ is the frequency detuning of the probe laser from the atomic resonance. Noting that $I=P/A$, where A is the area of the circular probe beam, rearranging Eq. (8) gives

$$\frac{dP}{P} = -\frac{N}{A} \left(\frac{\Gamma h\nu_L}{2I_{\text{sat}}} \right) = -n_1 \left(\frac{\Gamma h\nu_L}{I_{\text{sat}}\pi r} \right), \quad (9)$$

where $A = \pi r^2$, $n_1 = N/(2r)$ is the linear number density of atoms, and r is the probe-beam radius. Thus, the number of atoms emitted from the MMOT per second is given by

$$\Phi = n_1 v_0 = \left(-\frac{dP}{P} \right) \left(\frac{I_{\text{sat}}\pi r}{\Gamma h\nu_L} \right) v_0. \quad (10)$$

Because the MMOT magnetic fields were actually on during the probe pulse, the peak absorption $(dP/P)_0$ is reduced due to line broadening caused by the Zeeman effect. To account for this effect, the following procedure was used. The relative absorption (dP/P) observed immediately after turn-on of the probe pulse was measured as a function of the probe-laser detuning $\delta = \nu_L - \nu_0$ (circles in Fig. 5). While the Zeeman effect moderately broadens the absorption line, it does not significantly affect the integral of the absorption line because the Larmor frequency of the atoms (≤ 500 kHz) is of order or less than the optical-pumping rate of the probe laser (~ 2 MHz on-resonance). Therefore, the absorption signal that would be measured if the magnetic field were off is given by a Lorentzian with 6 MHz FWHM linewidth and an area equal to that of the measured absorption line. This Lorentzian is shown by the dashed line in Fig. 5. The output flux of

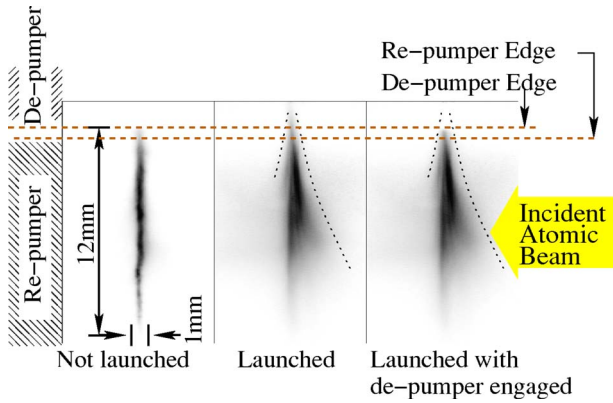


FIG. 6. (Color online) Fluorescence images of the MMOT (guide-axis vertical). The exposure times are chosen such that the images do not saturate. Left: launch velocity $v_0=0$ m/s. The fluorescence rapidly diminishes above the repumper knife edge. Middle: launch velocity $v_0=1.6$ m/s and depumping beam blocked. Atoms are transported upward out of the range of the MMOT, leaving a thin trail of fluorescence along the guide axis above the repumper edge. Right: launch velocity $v_0=1.6$ m/s and depumping beam active. The fluorescence abruptly diminishes above the depumper edge, as the depumper optically pumps all atoms into the dark state $F=1$. The dotted lines in the middle and right images outline a narrowing of the MMOT fluorescence as a function of height.

the MMOT is obtained by inserting the peak value of the Lorentzian $[-(dP/P)_0$ in Fig. 5] into Eq. (10). Typical obtained MMOT flux values are $\Phi_{\text{MMOT}}(v_0=2.2 \text{ m/s})=5.4 \times 10^8 \text{ s}^{-1}$ and $\Phi_{\text{MMOT}}(v_0=2.5 \text{ m/s})=4.8 \times 10^8 \text{ s}^{-1}$ for a MMOT field gradient of $\partial B/\partial \rho \approx 20 \text{ G/cm}$. Because of the uncertainty of the area under data curves like that shown in Fig. 5, we estimate the uncertainty of these flux values to be about 30%. The results indicate that the transfer efficiency from the primary PMOT atomic beam into the cold, concentrated beam emitted by the MMOT is 16%–18%. Further, the quoted MMOT flux values are a sum over all magnetic sublevels of the output atoms.

For MMOT's operated with gradients of $\partial B/\partial \rho = 15 \text{ G/cm}$ (225 A guide current) and $\partial B/\partial \rho = 10 \text{ G/cm}$ (150 A) we find MMOT flux values that are $\sim 90\%$ and $\sim 60\%$ of the above quoted ones, respectively. We further find that, while the average detuning δ_{MMOT} of our MMOT laser beams from resonance typically is of order two linewidths, the MMOT output flux does not vary significantly over a range of $-2.5\Gamma \lesssim \delta_{\text{MMOT}} \lesssim -1.5\Gamma$.

C. Dark-state extraction

Each atom emerging from the MMOT must traverse through the fringe fields of the four MMOT laser beams. This fact poses a problem, because accurate control of beam shapes and intensities in the fringe-field regions of the four MMOT beams is virtually impossible. Therefore, any extracted atom would experience strong, random differential radiation pressures in the fringe fields of the MMOT beams, causing the velocity to change in an erratic manner. The solution to this problem is dark-state extraction—i.e., optical

pumping of the atoms into a “dark state” that does not scatter any MMOT photons. The optical pumping into the dark state needs to occur inside the MMOT volume, *before* the atoms reach the fringe fields of the MMOT laser beams. As explained in [19], the location of optical pumping into the dark state is defined through a layered arrangement of a MMOT repumper beam with a well-defined upper knife edge and a depumper beam with a well-defined lower knife edge. Any overlap between the repumper and depumper beams needs to be avoided, while a small gap is allowable. The knife-edge planes are oriented orthogonal to the vertical guide axis. The MMOT repumper beam is resonant with the $^{87}\text{Rb } 5S_{1/2} F=1 \rightarrow 5P_{3/2} F'=2$ transition, while the depumper is resonant with the $5S_{1/2} F=2 \rightarrow 5P_{3/2} F'=2$ transition. This arrangement ensures that all atoms are transferred into the dark state $F=1$ after traversal of the depumper knife edge. Statistically, approximately one-third of the dark-state atoms will exit the MMOT in the magnetically guided sublevel $|F=1, m_F=-1\rangle$.

Fluorescence images of the MMOT in launch mode show a characteristic narrowing shape, indicated by the dotted lines in Fig. 6. As the atoms travel upward along the extraction trajectory, their transverse excursions away from the guide axis diminish. The narrowing reflects the progression of laser cooling into the moving reference frame of the MMOT as a function of height in the guide. Thus, optimal operation of the MMOT shows a chevronlike pattern where the tip is completely narrowed, indicating optimal cooling in the transverse directions at the extraction point.

Also characteristic in these images is that fluorescence is absent (left image) or diminished (middle image) above the repumper cutoff. This reflects off-resonant optical pumping of the atoms into the dark extraction state $F=1$ once they have left the range of the repumper beam. We have found that a small fraction of the atoms can be extracted from the MMOT in the dark state $F=1$ just by ensuring that the upper edge of the repumping region is located well within the MMOT region, as in the middle image. The flux of atoms extracted in the dark state is drastically improved by employing the depumper beam, as in the right image of Fig. 6. The sharp fluorescence cutoff at the lower edge of the depumper beam, seen in the right image, shows that all atoms still reaching the depumper region in the bright $F=2$ state are transferred into the $F=1$ dark extraction state by rapid on-resonant optical pumping. We have found experimentally that the presence of the depumping beam increases the yield of guided atoms by at least a factor of 5 over the yield obtained in the absence of the depumper (this contrast is relevant in Fig. 11 below).

IV. GRAVITATIONAL SLOWING AND MAGNETIC COMPRESSION

The vertical launch section of the guide has a height of 0.2 m from the depumper knife edge to the top end of the 90° bend. In the launch section, the atoms are slowed down by gravity as they travel upward. Using the MMOT laser frequencies as a velocity tuning parameter, the MMOT extraction velocity v_0 is adjusted such that the atomic flow has a reasonably low velocity at the top of the launch section

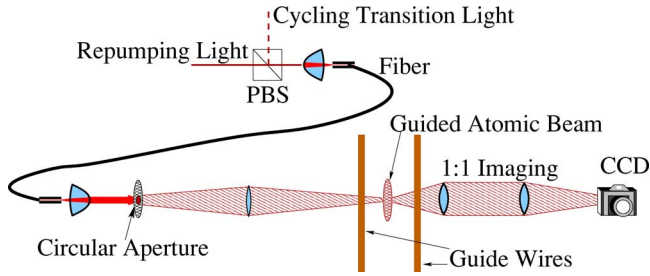


FIG. 7. (Color online) Experimental setup to probe the atomic beam with a top-hat intensity profile. The output of a fiber containing both repumper and cycling-transition light is collimated and directed onto a small aperture of <1 mm diameter. A long-focal-length lens images the top-hat intensity profile created at the aperture into the detection region. Fluorescence from the atomic sample is then observed using a one-to-one imaging scheme with a scientific charge-coupled-device (CCD) camera.

while maintaining a high atomic flux. We have found a useful extraction velocity range of $2.2 \text{ m/s} \leq v_0 \leq 2.8 \text{ m/s}$, corresponding to a velocity range $1 \text{ m/s} \leq v \leq 2 \text{ m/s}$ near the top end of the 90° bend.

The atom guide is tapered [20,21]; i.e., the center-to-center distance between the inner pair of guide tubes decreases from about 3.7 cm at the location where cold atoms are transferred from the MMOT into the guide down to 5.17 mm in the 90° bend. Taking the fields of both the inner and outer tube pairs into account, from Eq. (7) it follows that the field gradient increases from about 20 G/cm at the MMOT to 1.7 kG/cm in the 90° bend. A crucial benefit of the gradient increase is that the atomic distribution becomes magnetically compressed in the transverse directions as the atoms propagate through the tapered region. The compression enhances the collision rate and will thus, in the future, facilitate evaporative cooling.

Under the absence of collisions, the action of the transverse motion of the magnetically guided atoms, $S_\perp = \oint \mathbf{p}_\perp \cdot d\mathbf{q}_\perp$, is adiabatically conserved [20,21]. The adiabatic invariance entails a partial conversion of forward kinetic energy into transverse energy in the magnetic-compression region. Consequently, atoms in the vertical launch section of the guide are decelerated due to gravity and an additional retarding force that grows with increasing transverse energy. Simulations show that due to this effect, about half the atoms in the magnetically guided state $|F=1, m_F=-1\rangle$ are reflected backward. The reflected atoms are partially recycled, because they fall back into the MMOT. It is also noted that an increased collision rate will break the adiabatic conservation of the transverse action and, therefore, reduce the fraction of reflected atoms.

Once in the narrow region of the vertical guide section (5.17-mm center-to-center wire separation), additional velocity filtering occurs due to gravity and the 90° bend. While the fastest atoms overshoot the bend, the slowest atoms fall back into the MMOT. From simulations, we expect this filtering to further reduce the flux by about 15%.

The total coupling efficiency from the MMOT into the horizontal guide section is given by the fraction of atoms that exit the MMOT in the magnetic sublevel $m_F=-1$ (33%) times the probability that an atom does not fall back in the

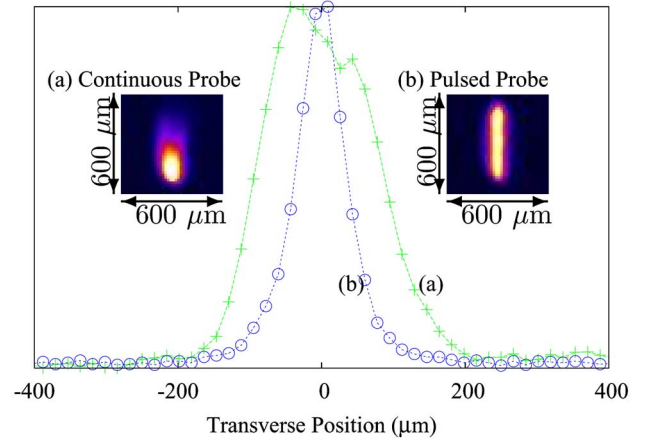


FIG. 8. (Color online) Fluorescence images (insets) and profiles transverse to the guide axis (curves) of a continuous atomic beam in the magnetic guide. In the images, the guide axis is vertical. The image obtained with continuous illumination [curve and inset (a)] is distorted and broadened due to radiation pressure and magnetic forces acting while the atoms are being imaged. The strobed image [curve and inset (b)] is much narrower and exhibits a constant fluorescence intensity along the full length of the illumination region along the guide axis. These properties of the strobed image follow from the fact that the strobe intervals are sufficiently short that no significant atomic motion occurs while the atoms are being imaged.

vertical guide section or overshoot in the bend (40%–50%). Thus, an initial estimate of the flux into the horizontal guide section is $\Phi_{\text{Hor}} = 0.15 \Phi_{\text{MMOT}} = 8 \times 10^7 \text{ s}^{-1}$.

V. ATOMIC-BEAM ANALYSIS BEFORE WAVEGUIDE BEND

A. Detection modes

We have first analyzed the atomic flow at the location where the vertical injection and launch section connects to the 90° bend. We use probe laser beams introduced approximately at a right angle relative to the vertical guide axis. Since the guided atoms are in the dark state $|F=1, m_F=-1\rangle$, bright fluorescence images require *two* laser beams, namely a repumping beam tuned to the $F=1 \rightarrow F'=2$ transition and a probe beam tuned to the $F=2 \rightarrow F'=3$ cycling transition. As shown in Fig. 7, the repumper and probe laser beams are merged into a common single-mode fiber. To minimize probe-light scattering on the guide tubes and to achieve well-defined beam intensities in the detection volume, the fiber output is collimated and directed onto an aperture of <1 mm diameter, such that the intensity variation of the beam profile immediately behind the aperture plane is negligible. Using a long-focal-length lens, the aperture is imaged into the detection volume, creating a circular probe region of about 1 mm in diameter with a top-hat intensity profile. The fluorescence of the atoms in that probe region is then observed using a scientific CCD camera.

To eliminate effects of Zeeman shifts, it is common practice to switch off magnetic fields before performing measurements. In the present experiment, where the time to reach steady state is on the order of several seconds, such a

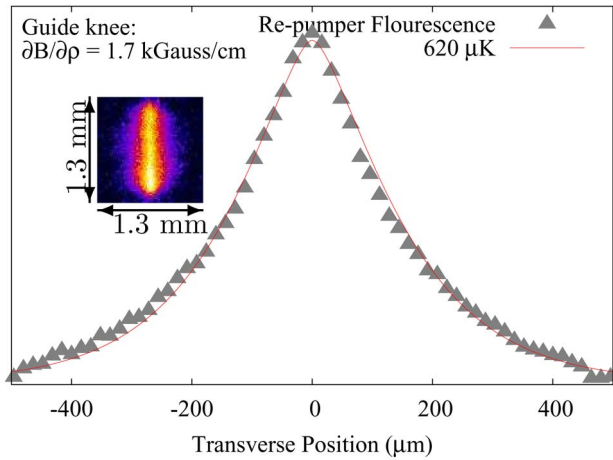


FIG. 9. (Color online) Atomic-beam image (inset) and corresponding profile transverse to the guide axis (data points). The image is obtained at a location just below the atom-guide knee with repumping light only. In the image, the guide axis is vertical. The line through the data points represents a fit for a temperature of $620 \mu\text{K}$.

magnetic-field-switching scheme would prescribe very low measurement repetition rates. Therefore, we have developed beam analysis methods that are compatible with continuous-mode atomic-beam operation, with the guide field always on. Consequently, Zeeman shifts need to be considered in the image analysis.

The most straightforward way to observe the atoms is to continuously illuminate the dark-state atomic flow with both the repumping and probe beams. As a result, a bright, continuous atomic-flow image is obtained [curve and inset (a) in Fig. 8]. Due to its simplicity, this real-time observation method is very useful when optimizing the PMOT and MMOT conditions for maximal atomic flow. However, it is noted that magnetic forces and radiation-pressure forces pull the atomic flow apart as soon as the atoms enter the illumination region. Therefore, images obtained with continuous probe light are distorted and much wider than the unperturbed atomic flow itself.

To obtain undistorted images of the atomic flow, the flow is probed in a strobed mode (i.e., continuous atomic beam, but pulsed detection). The light pulses are typically $20 \mu\text{s}$ long and therefore short enough that no distortion occurs during the brief illumination period. The separation between pulses is typically 1 ms, which is long enough that at each probe pulse the previously probed atomic-beam segment has cleared the detection volume and an unperturbed new atomic-flow segment has filled the detection volume. By accumulating many strobed probe measurements, undistorted images of the atomic beam can be obtained [curve and inset (b) in Fig. 8]. Using a nonamplified CCD camera, we typically integrate over 1000 strobed images.

B. Measurement of the transverse temperature

In the following, we use the term “temperature” in order to quantify the velocity spread of the atoms, even though the

collision rate is too small to establish a local thermal equilibrium in the atom flow. This deliberate use of the term temperature is common in laser-cooling applications.

The most direct method to measure the transverse temperature is to only use repumper light in the probe region, with an intensity exceeding about one saturation intensity of the cycling transition ($I_{\text{sat}} = 1.6 \text{ mW}/\text{cm}^2$). The duration of the strobe intervals ($20 \mu\text{s}$) is sufficiently long that all atoms inside the detection volume scatter of the order of two repumper photons and become optically pumped into the $F = 2$ state. Notably, this even applies to atoms traveling in the wings of the atomic flow, which experience the largest Zeeman shifts. Each atom in the probe volume therefore produces the same amount of fluorescence signal during detection, independent of the magnetic field at which the atom is located. Due to this uniformity of the signal obtained per atom, images obtained with only repumper light are proportional to the atomic-flow density projected onto the image plane. This property makes repumper-only images particularly easy to analyze. A slight disadvantage of repumper-only images is that the low total photon yield per atom, only of order 2, leads to dim images.

A typical repumping-only fluorescence image and its profile are displayed in Fig. 9. Assuming a thermal distribution in the degrees of freedom x and y transverse to the guide axis, the profile data can be fitted with a function

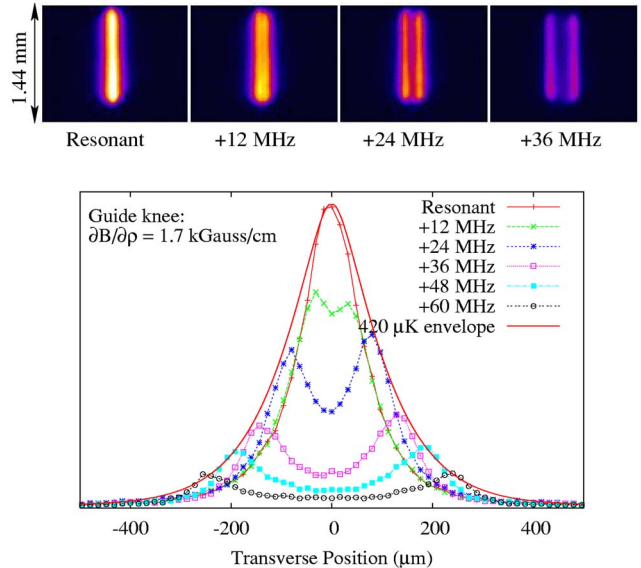


FIG. 10. (Color online) Top row: atomic-beam images with both repumper light and probe light present in the detection region for the indicated detunings of the probe laser relative to the field-free transition frequency. The images are obtained at a location just below the atom-guide knee and with a horizontal linear polarization of the probe laser. In the images, the guide axis is vertical. Lower panel: profiles of atomic-beam images transverse to the guide axis for the indicated detunings of the probe laser relative to the field-free transition frequency. By fitting the *envelope* of the profiles with curves of the type of Eq. (12), a transverse temperature of $T_{\perp} \approx 420 \mu\text{K}$ is obtained.

$$P(x) \propto \int_{-\infty}^{\infty} \exp\left[-\frac{V(x,y)}{k_B T_{\perp}}\right] dy, \quad (11)$$

where the magnetic-dipole potential $V(x,y) = \frac{1}{2}\mu_B B(x,y)$ and μ_B is the Bohr magneton. $B(x,y)$ is the exact magnetic field for a pair of infinitesimally thin wires separated by the center-to-center distance of the guide wires. A small longitudinal component (≈ 200 mG) generated by a combination of the Earth's magnetic field and other environmental fields is also present. The transverse temperature T_{\perp} is the fit parameter of interest. The data in Fig. 9 are fit best with $T_{\perp} = 620 \mu\text{K} \pm 15 \mu\text{K}$.

If the atoms are illuminated with both repumper and probe light, the fluorescence on the cycling transition entirely dominates the photon yield per atom. Using a probe intensity of the order of ten saturation intensities, atoms located at a magnetic field at which the applied probe light is resonant with the cycling transition scatter the order of 300 photons during a strobe pulse of $20 \mu\text{s}$ duration. By detuning the frequency of the probe light, the Zeeman shift 1.4 MHz/G of the cycling transition $|F=2, m_F=2\rangle \rightarrow |F'=3, m'_F=3\rangle$ manifests itself as shown in Fig. 10: for zero detuning of the probe laser from the field-free transition frequency, mostly atoms traveling very close to the guide axis, where the magnetic field is low, are observed. For significant detunings, the images mostly show atoms traveling at a distance from the guide axis where the magnetic field is such that the cycling transition is resonant. The signal from these outlying atoms depends strongly on the polarization of the probe light. To balance optical pumping effects on both sides of the guide axis in the image plane, a linear probe light polarization was used. Taking multiple atomic-beam profiles at different detunings (and equal intensities), the *envelope* of the entire set of curves gives a representation of the transverse extension of the atomic beam. Assuming a thermal distribution in the transverse degrees of freedom, the transverse temperature T_{\perp} can be determined by fitting the envelope to the function

$$P_E(x) \propto \int_{-\infty}^{\infty} w(x,y) \exp\left[-\frac{V(x,y)}{k_B T_{\perp}}\right] dy, \quad (12)$$

where $w(x,y)$ is the position-dependent number of photons scattered per atom. For a linear probe-laser polarization transverse to the guide axis, the probed atoms tend to be optically pumped into the magnetic sublevels $|F=2, m_F = \pm 2\rangle$ (quantization axis parallel to the laser direction). Thus, approximately half of the probe-light intensity I drives the atoms on the cycling transition and $w(x,y)$ is given by

$$w(x,y) = \frac{\Gamma}{2} \frac{s}{(s+1)} \tau, \quad (13)$$

where Γ is the excited-state decay rate ($2\pi \times 6 \text{ MHz}$), τ is the strobe interval, s is given by

$$s = \frac{I}{2I_{\text{sat}}} \frac{1}{1 + 4[2\pi\delta(x,y)/\Gamma]^2}, \quad (14)$$

and

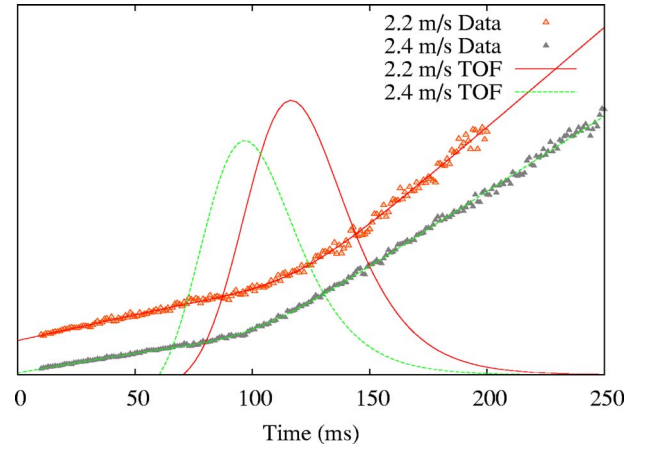


FIG. 11. (Color online) Time-of-flight experiment in the vertical launch section. The time-integrated atomic-beam fluorescence (triangles) is shown vs the integration time for the indicated launch velocities. At time zero, the atomic flux out of the MMOT is suddenly increased by about a factor of 5. The time-of-flight distributions (curves peaking at about 100 ms) are obtained by twice differentiating the smoothed curves laid through the data points.

$$\delta(x,y) = \frac{\mu_B}{h} [B(x,y) - B(x,0)] \quad (15)$$

is the detuning of the probe laser from the Zeeman-shifted atomic resonance at location $(x,0)$. Note that the fitting function in Eq. (12) does not represent a profile for a single laser frequency. Rather, Eq. (12) represents the envelope of the peaks from a set of profiles obtained with different laser frequencies. Using fit functions of the type in Eq. (12), the envelope of the data in Fig. 10 is found to correspond to a transverse temperature $T_{\perp} \approx 420 \mu\text{K}$.

In all measurements where the frequency of the probe laser was varied and the temperature T_{\perp} was obtained by fitting the envelope of the peaks in the fluorescence profiles (such as in Fig. 10), the fit results for T_{\perp} were notably lower than those found using the repumper-only scheme. This discrepancy is explained as follows. Since the repumper frequency was not detuned with the probe, the repumping rates in the wings of the atomic beam were notably lower than those near the core of the atomic distribution. Thus, atoms in the wings require a significant fraction of the probe-pulse duration to become repumped and produce less net fluorescence on the cycling transition than atoms traveling near the guide center. This effect leads to systematically reduced values for T_{\perp} in the temperature fits. Therefore, temperatures obtained using the repumper-only scheme (as in Fig. 9) are considered more reliable than those obtained with the probe-repumper scheme (as in Fig. 10).

C. Measurement of the longitudinal temperature

To determine the longitudinal temperature of the guided atomic beam, we have performed a time-of-flight analysis. This was done by observing the turn-on behavior of the atomic-beam density after a sudden enhancement of the atom flow out of the MMOT. The atomic flow is suddenly enhanced by about a factor of 5 by turning on the depumping

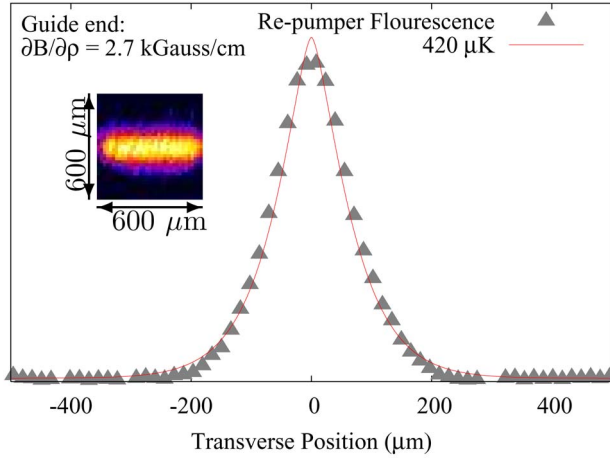


FIG. 12. (Color online) Atomic-beam image obtained at the end of the atom guide with repumping light only (inset) and corresponding profile transverse to the guide axis (data points). In the image, the guide axis is horizontal. The line through the data points represents a fit for a temperature of $420 \mu\text{K}$.

beam located in the MMOT exit region. The data were obtained by varying the time over which the atomic-beam fluorescence is integrated. Data sets for two different launch velocities, displayed in Fig. 11, show that the signal varies linearly with integration time until the enhanced atomic flow reaches the probe region, at which point the slope changes due to the increase in atomic flux. The time-of-flight distribution is obtained by differentiating the curves shown in Fig. 11 twice.

Neglecting magnetic retardation effects [21] in the compression region of the magnetic guide, it is straightforward to convert the time-of-flight curves in Fig. 11 into a distribution of velocities at the observation point. The corresponding estimate for the longitudinal temperature T_{\parallel} of the atoms is found to be $T_{\parallel} \sim 900 \mu\text{K}$. Since the retardation depends on

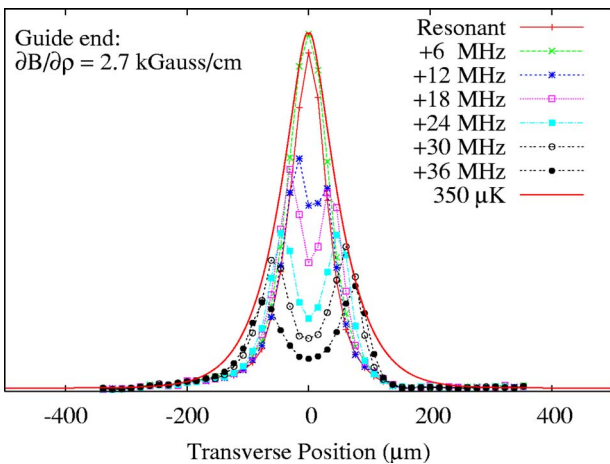


FIG. 13. (Color online) Profiles of atomic-beam images transverse to the guide axis with both repumper light and probe light present in the detection region for the indicated detunings of the probe laser relative to the field-free transition frequency. The estimate $T_{\perp} \approx 350 \mu\text{K}$ is obtained by fitting the *envelope* of the profiles with curves of the type from Eq. (12).

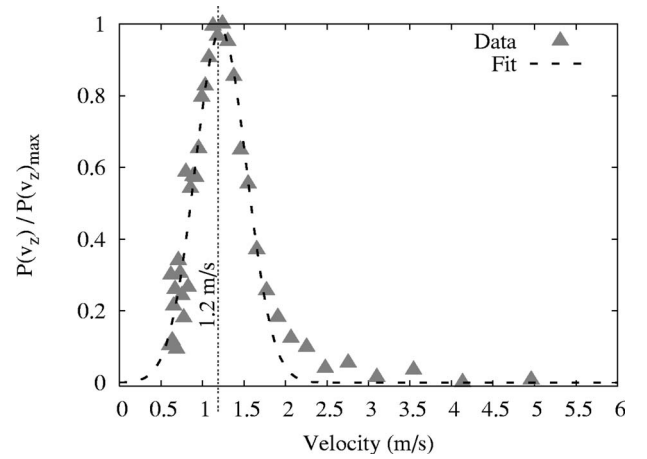


FIG. 14. Longitudinal velocity distribution obtained from a time-of-flight experiment in the horizontal section of the atom guide. The MMOT launch velocity is $v_0 = 2.2 \text{ m/s}$. The velocity distribution yields a longitudinal temperature of $\approx 1 \text{ mK}$ and an average forward velocity of $\approx 1.2 \text{ m/s}$.

the transverse energy distribution [21], it broadens the time-of-flight signal relative to the signal one would obtain without retardation. Thus, the estimate $T_{\parallel} \sim 900 \mu\text{K}$ provides an upper limit of the actual value T_{\parallel} . We have performed simulations in which the exact guide fields were used and thus retardation effects were fully accounted for. Assuming MMOT temperatures $T_{\parallel} = 300 \mu\text{K}$ and $T_{\perp} = 250 \mu\text{K}$ ($T_{\perp} = 150 \mu\text{K}$ is the Doppler limit for Rb), the simulations yield $T_{\parallel} = 890 \mu\text{K}$ in the probe region, which is compatible with the experimentally obtained upper limit.

It is noted that in our current MMOT configuration a value of T_{\perp} greater than the Doppler limit is expected. Images of the MMOT, such as those shown in Fig. 6, typically show incomplete narrowing of the atomic beam at the extraction point of the MMOT. As discussed in Sec. III C, this observation indicates less than optimal cooling in the transverse directions.

VI. ATOMIC-BEAM ANALYSIS AT THE END OF THE ATOM GUIDE

A. Measurement of the transverse temperature

The vertical injection and launch section of the guide is connected with the 1.5-m-long horizontal section via a 90° bend with a radius of 1 in. Considering this geometry as well as the centrifugal force and the transverse gradient of the atom guide in the bend region, it is found that atoms with launch velocities in the range $2 \text{ m/s} < v_0 < 3.8 \text{ m/s}$ will be able to transit into the horizontal guide section. Experimentally, a smaller useful range of $2.2 \text{ m/s} < v_0 < 2.8 \text{ m/s}$ is found. We believe that on the low-velocity side the useful v_0 range is limited by the reflection of slow atoms in the magnetic-compression region [21], while on the high-velocity side it is caused by limitations in the MMOT operation. In view of the long-term goals of our work, we are mostly interested in the low-velocity end of the useful v_0 range.

In the horizontal guide section, the center-to-center distance between the guide tubes linearly decreases from 5.18 mm after the bend to 4.18 mm at the end. Thus, at 300 A guide current the magnetic-field gradient increases from 1.7 kG/cm to 2.7 kG/cm, leading to a further moderate adiabatic compression of the atom flow.

Using the same methods as described in Sec. V B, atomic-beam images and corresponding temperature fits have been performed at the end of the guide. Fitting the data from a repumper-only measurement, as shown in Fig. 12, with functions of the type of Eq. (11), we find a transverse temperature $T_{\perp} = 420 \mu\text{K} \pm 40 \mu\text{K}$. Also, as shown in Fig. 13, a temperature fit of $T_{\perp} = 350 \mu\text{K}$ was determined by the probe-repumper-type measurement. Following the discussion in Sec. V B, the temperature obtained with the probe-repumper method is considered less reliable.

B. Measurement of the longitudinal temperature

In the horizontal section of the guide, a time-of-flight experiment has been performed. At a location 50 cm ahead of the detection region, a laser beam tuned to the repumping transition ($F=1 \rightarrow F'=2$) is introduced. This beam is on most of the time and strongly attenuates the atomic beam. An interruption of this repumper beam for 50 ms defines a short pulse of guided atoms that is allowed to propagate through the length of the guide into the probe region located at the end of the guide. By measuring the temporal spread of the atom pulse, the longitudinal velocity distribution of the atomic beam is derived. A typical result is shown in Fig. 14. Fitting the velocity distribution with functions of the type

$$P(v) \propto \exp\left[-\frac{M(v-v_c)^2}{2k_B T_{\parallel}}\right],$$

we find, for the case displayed in Fig. 14, a longitudinal temperature of $T_{\parallel} \approx 1 \text{ mK}$ and an average forward velocity of $v_c \approx 1.2 \text{ m/s}$. Since in this measurement the tapering of the atom guide and the resultant magnetic retardation force [21] along the time-of-flight stretch was minimal, the values of T_{\parallel} and v_c are reliable.

C. Temperature changes along the guide

In the following, the changes in transverse temperature that occur along the guide are discussed. The first notable change in temperature occurs between the MMOT and upper end of the magnetic-compression zone in the vertical launch section of the guide. While maintaining the phase-space density of the atoms, the compression has the side effects of retarding their forward motion and heating them both transversely and longitudinally. In a trajectory simulation in which temperatures of $T_{\parallel} = 300 \mu\text{K}$ and $T_{\perp} = 250 \mu\text{K}$ at the exit of the MMOT are assumed, the transverse temperature shows an increase to T_{\perp} to $600 \mu\text{K} \pm 40 \mu\text{K}$ at the observation point used in Sec. V B (the error bar arises from statistical noise in the simulation). This simulation result is in reasonable agreement with the experimental result.

The results of Secs. V B and VI A further indicate a considerable decrease in T_{\perp} between the respective observation

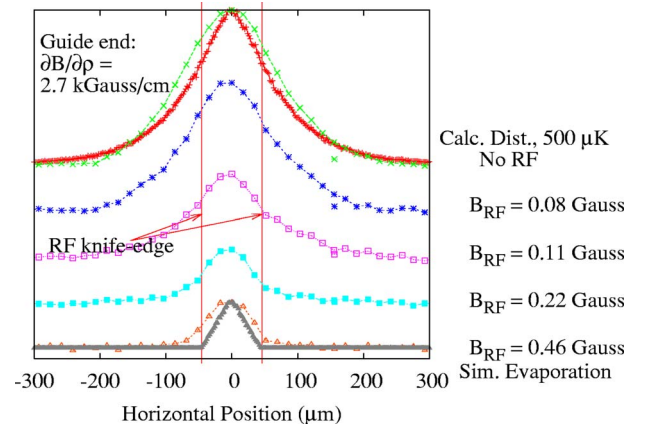


FIG. 15. (Color online) Atomic-beam profiles transverse to the guide axis at the end of the atom guide, obtained with repumping light only and with a continuous radio-frequency (rf) current of 9 MHz frequency. The rf current is coupled onto a guide tube in the horizontal guide section. The estimated value of the rf-field magnitude, B_{RF} is indicated to the right of the plot. The experimental data agree reasonably well with calculations for a thermal distribution with $T_{\perp} = 500 \mu\text{K}$ (red curve) and the same thermal distribution truncated at the “rf knife edge” (gray curve). Both theoretical curves are scaled with the same factor to match the experimental data.

points. This decrease is a secondary consequence of magnetic compression. Since the action of the transverse motion is adiabatically conserved, during the compression longitudinal energy becomes partially converted into transverse energy [21]. Thereby, the amount of energy that is converted increases with increasing transverse energy. Due to this interdependence, the longitudinal velocity distributions and the transverse positions in Figs. 9 and 12 are not independent. The further off axis an atom travels, the slower it is longitudinally. Since between the observation points of Figs. 9 and 12 the atoms undergo a final 1.6-cm vertical climb, the farther out an atom is in Fig. 9, the higher the chance that it does not make the climb and falls back into the MMOT. Thus, there is a trend that between the observation points of Figs. 9 and 12 the outermost atoms fall back. This effect causes the transverse temperature to decrease. Simulations show that the transverse temperature decreases from $T_{\perp} \approx 600 \mu\text{K}$ to $425 \mu\text{K} \pm 35 \mu\text{K}$ during the final 1.6 cm of vertical climb. This simulation result agrees well with the experimentally observed temperature drop.

VII. FLUX MEASUREMENT

Using atomic-beam images obtained with the repumper only, a measurement of the atomic flux in the guide has been performed. The method relies on the fact that the total photon yield per atom for repumper light is quite well known (simulations show about two photons per atom). Important parameters entering into the calculation are the geometric collection efficiency of the camera lens, as well as the pixel yield of the camera per photon reaching the CCD chip.

An analysis along these lines for a launch velocity of 2.5 m/s has yielded an atomic flux of $1.9 \times 10^7 \text{ s}^{-1}$ and a

central volume density of about $1.2 \times 10^9 \text{ cm}^{-3}$ at the end of the guide, with uncertainties less than a factor of 2. The s -wave elastic collision rate (cross section $\sigma=700 \text{ nm}^2$) at this density and at a temperature of $500 \text{ } \mu\text{K}$ is about 0.5 per second, corresponding to about one elastic collision of any given atom during its passage through the atom guide. Therefore, under the present conditions collisions will barely affect the dynamics of the atomic flow and of rf-induced atom removal, discussed in the next section.

The flux measured at the end of the guide amounts to approximately 4% of the MMOT output flux. This result is about a factor of 4 less than our initial estimate at the end of Sec. IV. We attribute this disparity to the depleting effect of stray repumper light in the vertical section of the guide, which optically pumps atoms from the guided state $|F=1, m_F=-1\rangle$ into other states. We have found very recently that this effect can be alleviated by detuning the repumper laser that is coupled into the MMOT region. Using a detuned repumper, a flux increase of about a factor of 5 at the end of the guide was observed.

VIII. CONTINUOUS rf-INDUCED ENERGY-SELECTIVE REMOVAL OF ATOMS

An rf current is coupled onto one of the guide tubes in the horizontal guide section. Since most of the rf-induced magnetic field is confined to the region between the tubes, this rf-coupling scheme requires little rf power and minimizes rf interference. The rf magnetic field is transverse to the guide axis and has a component transverse to the local static magnetic field practically everywhere on the evaporation surface. rf-induced removal of atoms from atom guides has been performed previously using a different antenna geometry [22,23].

Figure 15 shows profiles of the atomic beam at the end of the guide for continuously applied rf currents at a frequency of 9 MHz and the indicated estimated values of the rf magnetic-field amplitude. At 9 MHz rf frequency, a large portion of the atomic beam is above the evaporation threshold $2\pi\hbar \times 9 \text{ MHz}$ (=the “rf knife edge”) and should become removed if the rf-coupling scheme is effective. Figure 15 shows that an applied rf field of $B_{\text{RF}}=500 \text{ mG}$ is sufficient for continuous rf-induced removal of practically all atoms above the “rf knife edge.” In the figure, we also compare the measured fluorescence profiles with a fit for a thermal distribution function ($T_{\perp}=500 \text{ } \mu\text{K}$, red curve in Fig. 15) and the same distribution truncated at an energy of $2\pi\hbar \times 9 \text{ MHz}$. There is reasonably good agreement between the calculated curves and the respective measured profiles with no rf and $B_{\text{RF}}=500 \text{ mG}$.

It is noted that the experimental curves are wider than the calculated ones by $\sim 20 \text{ } \mu\text{m}$. The experimental broadening is due to diffraction effects and image smearing associated with the camera pixel size. Integrating the experimental data in Fig. 15, it is found that 16% of the atoms are left after energy-selective removal of atoms exceeding a transverse energy of $2\pi\hbar \times 9 \text{ MHz}$. Using a calculation, the average potential energy of the atoms remaining after the rf-induced atom removal is found to equal $\approx 11\%$ of the average potential energy without rf-induced atom removal.

IX. DISCUSSION

We have realized a continuous flow of atoms in a 1.7-m-long magnetic atom guide and measured longitudinal and transverse temperatures of the guided atomic beam. Continuous rf-induced removal of the most energetic atoms from the guide has been demonstrated. There is no evidence that elastic collisions play a role in the observed atomic-flow dynamics.

The long-term goal of this project is to generate a continuous-wave, amplitude- and phase-stable coherent atomic beam extracted from a continuous-wave Bose-Einstein condensate (cw-BEC), which will be the ideal atom source to operate atom-interferometric devices. It has been proposed [12,13,24,25] to produce quantum-degenerate atomic beams via forced evaporative cooling in long magnetic guides. The work presented in this paper lays important foundations for the realization of these ideas. Related work performed at ENS, Paris [22] has now recently resulted in the demonstration of evaporative cooling in a magnetic guide [23]. In this context, the next step in this project will be to demonstrate single-frequency rf-induced evaporative cooling in the horizontal section of the guide. The challenge will be to obtain collision rates high enough that the atom evaporation causes a strong increase in the phase-space density of the atomic beam. Several modifications are planned to achieve this goal, including the following. Active control over the longitudinal magnetic field as a function of longitudinal position will be introduced, allowing a position-dependent evaporation threshold with a single rf frequency. The MMOT will be modified into a longitudinally compressed MMOT where the field gradient increases from $\sim 20 \text{ G/cm}$ to $\sim 200 \text{ G/cm}$ within the MMOT light field. From simulations of this compressed MMOT, we expect an increase of initial phase-space density and collision rates by a factor of 10. We also expect that the coupling from the MMOT into the horizontal guide section will improve after implementation of a compressed MMOT. The MMOT will also be increased in length to allow sufficient time for optimal cooling. Further, it is planned to replace the PMOT by a Zeeman slower, which is expected to increase the atom flux by about a factor of up to 100 relative to present values.

To further evaluate the currently achieved performance, we calculate the number of quantum-mechanical atom-guide modes in the plane transverse to the guide axis via a semi-classical analysis in cylindrical coordinates. The number of modes with an outer turning point less than ρ_0 is given by

$$N_{\text{modes}} = \sum_{m=-\infty}^{\infty} \frac{2}{h} \int_{\rho_{\text{min}}}^{\rho_0} \sqrt{2M[E_m(\rho_0) - E_m(\rho)]} d\rho,$$

where the potential energy

$$E_m(\rho) = \frac{\hbar^2(m^2 - 1/4)}{2\rho^2} + \left| \frac{\partial B}{\partial \rho} \mu_B g_F \right| \rho,$$

the angular momentum about the guide axis $l_z = \hbar m$, and ρ_{min} is defined via $E_m(\rho_{\text{min}}) = E_m(\rho_0)$ (let $\rho_{\text{min}} \rightarrow 0$ for $m=0$). To estimate the number of modes that carry a significant flow, from Fig. 15 we estimate, for the case where no rf is applied, $\rho_0 = 100 \text{ } \mu\text{m}$ and obtain $N_{\text{modes, no rf}} = 3.5 \times 10^8$, while for the

case of rf-induced energy filtering we estimate $\rho_0=40 \mu\text{m}$ and obtain $N_{\text{modes,with rf}}=3.6 \times 10^7$. Assuming that the atom flux is the same in all significant guide modes, the flux per mode is about $\Phi_1=0.2 \text{ s}^{-1} \text{ mode}^{-1}$. Assuming that one were to build an atom interferometer based on filtering the atomic beam in a way that only the fundamental guide mode enters the interferometer, this flux per mode would correspond to the count rate. Reasonable experiments will require a count rate of order 10^3 s^{-1} . Therefore, an increase of the phase-space density by a factor of the order of 10^4 , combined with mode-filtering techniques, will be sufficient to perform atom-interferometric experiments in the guide. This increase could be obtained by implementing a larger initial flux, using, for instance, a Zeeman slower, and some degree of evaporative cooling enabled by an improved collision rate. Further,

the present phase-space density, estimated to be $h\Phi_1/(M\Delta v_z \langle v_z \rangle) \sim 10^{-9}$, needs to be increased by a factor of the order of 10^9 to reach a quantum-degenerate atomic flow. We believe that this factor can be reached by evaporative cooling, after increasing the initial atomic flux and the atom density using a Zeeman slower, and by using an improved, compressed MMOT for atom injection into the guide.

ACKNOWLEDGMENTS

This work was supported by the Army Research Office and the Office of Naval Research (Project No. 42791-PH), the National Science Foundation FOCUS Center, and the Michigan Center for Theoretical Physics.

-
- [1] S. Wildermuth, S. Hofferberth, I. Lesanovsky, E. Haller, L. M. Andersson, S. Groth, I. Bar-Joseph, P. Krüger, and J. Schmiedmayer, *Nature (London)* **435**, 440 (2005).
- [2] J. M. McGuirk, G. T. Foster, J. B. Fixler, M. J. Snadden, and M. A. Kasevich, *Phys. Rev. A* **65**, 033608 (2002).
- [3] T. L. Gustavson, P. Bouyer, and M. A. Kasevich, *Phys. Rev. Lett.* **78**, 2046 (1997).
- [4] J. Schmiedmayer, M. S. Chapman, C. R. Ekstorm, T. D. Hammond, S. Wehinger, and D. E. Pritchard, *Phys. Rev. Lett.* **74**, 1043 (1995).
- [5] Y. Shin, C. Spanner, G.-B. Jo, T. A. Pasquini, M. Saba, W. Ketterle, D. E. Pritchard, M. Vengalattore, and M. Prentiss, e-print cond-mat/0506464 v2.
- [6] M. A. Kasevich, *Science* **298**, 1363 (2002), and references therein.
- [7] G. Zabow, R. S. Conroy, and M. G. Prentiss, *Phys. Rev. Lett.* **92**, 180404 (2004).
- [8] K. I. Lee, J. A. Kim, H. R. Noh, and W. Jhe, *Opt. Lett.* **21**, 1177 (1996).
- [9] E. L. Raab, M. Prentiss, A. Cable, S. Chu, and D. E. Pritchard, *Phys. Rev. Lett.* **59**, 2631 (1987).
- [10] R. S. Williamson III, P. A. Voytas, R. T. Newell, and T. Walker, *Opt. Express* **3**, 111 (1998).
- [11] Z. T. Lu, K. L. Corwin, M. J. Renn, M. H. Anderson, E. A. Cornell, and C. E. Wieman, *Phys. Rev. Lett.* **77**, 3331 (1996).
- [12] P. Cren, C. F. Roos, A. Aclan, J. Dalibard, and D. Guéry-Odelin, *Eur. Phys. J. D* **20**, 107 (2002).
- [13] C. F. Roos, P. Cren, T. Lahaye, J. Dalibard, and D. Guéry-Odelin, *Laser Phys.* **13**, 605 (2003).
- [14] S. Weyers, E. Aucouturier, C. Valentin, and N. Dimarcq, *Opt. Commun.* **143**, 30 (1997).
- [15] K. Dieckmann, R. J. C. Spreeuw, M. Weidemüller, and J. T. M. Walraven, *Phys. Rev. A* **58**, 3891 (1998).
- [16] P. Berthoud, A. Joyet, G. Dudle, N. Sagna, and P. Thomann, *Europhys. Lett.* **41**, 141 (1998).
- [17] P. Berthoud, E. Fretel, and P. Thomann, *Phys. Rev. A* **60**, R4241 (1999).
- [18] J. Schoser, A. Batär, R. Löw, V. Schweikhard, A. Grabowski, Y. B. Ovchinnikov, and T. Pfau, *Phys. Rev. A* **66**, 023410 (2002).
- [19] B. K. Teo, T. Cubel, and G. Raithel, *Opt. Commun.* **212**, 307 (2002).
- [20] B. K. Teo and G. Raithel, *Phys. Rev. A* **63**, 031402(R) (2001).
- [21] B. K. Teo and G. Raithel, *Phys. Rev. A* **65**, 051401(R) (2002).
- [22] T. Lahaye, J. M. Vogels, K. J. Günter, Z. Wang, J. Dalibard, and D. Guéry-Odelin, *Phys. Rev. Lett.* **93**, 093003 (2004).
- [23] T. Lahaye, Z. Wang, G. Reinaudi, S. P. Rath, J. Dalibard, and D. Guéry-Odelin, *Phys. Rev. A* **72**, 033411 (2005).
- [24] E. Mandonnet, A. Minguzzi, R. Dum, I. Carusotto, Y. Castin, and J. Dalibard, *Eur. Phys. J. D* **10**, 9 (2000).
- [25] *Bulletin of the Research Corporation, Winter issue*, Research Corporation, Tucson, Arizona (1999).